arXiv:1407.2925v1 [cs.MS] 9 Jul 2014

A data porting tool for coupling models with different discretization needs

S.Ion*, D.Marinescu*, S.G.Cruceanu*, and V.Iordache†

June 24, 2014

Abstract

The presented work is part of a larger research program dealing with developing tools for coupling biogeochemical models in contaminated landscapes. The specific objective of this article is to provide the researchers a tool to build hexagonal raster using information from a rectangular raster data (e.g. GIS format), data porting. This tool involves a computational algorithm and an open source software (written in C). The method of extending the reticulated functions defined on 2D networks is an essential key of this algorithm and can also be used for other purposes than data porting. The algorithm allows one to build the hexagonal raster with a cell size independent from the geometry of the rectangular raster. The extended function is a bicubic spline which can exactly reconstruct polynomials up to degree three in each variable. We validate the method by analyzing errors in some theoretical case studies followed by other studies with real terrain elevation data. We also introduce and briefly present an iterative water routing method and use it for validation on a case with concrete terrain data.

Keywords: Raster data, interpolation, cubic polynomials, hexagonal raster, hydrological modelling, water routing.

*Institute of Statistical Mathematics and Applied Mathematics, Romanian Academy, Calea 13 Septembrie No. 13, 050711 Bucharest, Romania, Phone/Fax (4021)3182439, email: stelian.ion@ima.ro, dorin.marinescu@ima.ro, stefan.cruceanu@ima.ro.

†University of Bucharest, Research Center for Ecological Services, email: virgil.iordache@bio.unibuc.ro

1 Introduction

Predicting the long distance effects of local environmental changes requires a coupling between local and regional models of ecological and abiotic processes. Examples include the integration of local vegetation processes with regional transport models for heavy metals (e.g. [27, 28, 29] for reviews and general methodological steps), or the local resources development with movement of animal species (e.g. [24] for review of Partial Differential Equations (PDEs) used in spatial interactions and population dynamics, and [19] for an application using Geographic Information Systems (GIS)).

Direct coupling of the models is technically possible, but allows less flexibility for further model development. Alternatively, more common and flexible geographical objects are used as an interface among models of processes occurring at different space-time scales. One specific problem with this integration strategy is that the kind and properties of the geographical objects used as input to or output from local and regional models are usually different (see [55] for some examples of problems raised by integrated modelling). The differences arise due to methodological constraints related to the measurements of the space variables and to the modelling techniques. Table 1 summarizes the types of geographical objects which can occur (summarized and developed from [18]).

It can be seen from the inspection of this table that raster data and vector data are not basic terms in geographical ontology (see also [16]). For instance a raster refers in principle to a square tessellation of the plane with a constant value of the space variable function inside each square. Although raster data models are not a primary information source, in practical modelling they are frequently the only available primary data source scales (e.g. in digital terrain models). A large volume of GIS raster data is now-a-days collected and used for scientific research purposes, as well as for different practical applications, and a wide variety of software has been developed over time for reading and processing it [23, 3] (one may also see [53] for a practical guide to use public domain geostatistical and GIS software). The data of a raster are organized into rows and columns and structured as a matrix. Any information of interest is characterized by an unique value in each cell which maybe "null" if no data is available. This information may represent continuous data, as elevation, temperature, rainfall intensity or discrete (thematic, nominal) data, as land use or soil category, [23]. The fidelity of a raster data with respect to the real information is a challenging issue [11, 34, 36, 39, 48]

Table 1: Types of geographical objects occurring directly and indirectly in the modelling of coupled environmental process (reconstructed and adapted from [18]). Field type approach allows a rigorous description of the error and empirical verification, while discrete type approach does not allow a good treatment of errors, usually involves a filtering of empirical data.

Approach	Measurement, observation	Primary ("real") geographical objects	Derived ("methodological") geographical objects (resulted from data modelling and plane discretization)
Field type (properties with relation of spatial location)	Variables z - observable at a scale much smaller than the derived geographical objects and the empirical precision of geographical location Variables z - observable at a scale larger than the potentially derivable geographical objects and the empirical precision of geographical location	Tuples $< x, y, z_1, \ldots, z_n >$ with space variables z and location (x, y). Tuples with (x, y) on the observation polygon or on the transect line (e.g the center of the 50 x 50 m plot). Interpolated field (the infinite set of tuples).	Substrates with attributes (polygons, contour lines, regularly distributed points as centers of a plane discretization). The polygons are characterized by a variation of the variables inside them (a constant in the simplest case). The size of the polygons is not empirically constrained; Substrates with attributes. It makes no natural sense to have the size of the discretization units smaller than the observation scale of the spatial variables.
Discrete type (substrate located in space with properties)	The observation scale does not influence the approach. Usually this approach make use of old geographical maps or methodological objects resulted from field approach.	Points, polygons, lines filling and empty geographical space.	Field obtained by planar enforcement (points with a certain value inside the discrete object, by class, and a constant value in the empty space).

that must be taken into consideration since the errors propagate on raster data outputs [42, 54, 56]. Usually, large cells entail poor accuracy. Some mathematical models of environmental phenomena require information at a subgrid-scale. For example, the input data for partial differential equations must satisfy a certain degree of smoothness. Also, the domain discretization may be better suited to configurations other than that of common square cells. Such situations may appear when one uses finite volume or finite element methods to numerically solve PDEs, as well as when one uses models based on hexagonal cellular automata [1]. With the development of laser altimetry in geography and ecology ([31, 50]), point clouds tend to be more often used for direct analysis within a GIS. Hexagonal lattices can be used for the extraction of knowledge by clustering techniques from such data (e.g. [30, 20]). Using the rasters obtained by interpolations of LiDAR data, [40] have pointed out the important influence of DTM resolution on the estimated soil loss by erosion modelling. This influence could be explored also by erosion models using hexagonal lattices if the porting software would be available. In this context, one can say that there is a need to build spatial interpolation algorithms for the purpose of porting rectangular raster information to other networks with cells of a different size or geometry, i.e. a method of *data porting* (DP). These algorithms should be developed in such a way to preserve as much as possible the original measured space variables. In this article we tackle the particular situation of variables treated by a field type approach, observable at a scale much smaller than the derived geographical objects and the empirical precision of geographical location, having the size of the derived and not empirically constrained polygons. In particular, we present a DP method to construct a hexagonal raster using a rectangular raster data input. To the best of our knowledge and according to [57], there are currently no databases provided in "hexagonal raster format".

1.1 Data porting methods

A rough classification divides DP into one stage and multi-stage methods. In a one stage method, the data value corresponding to a cell c_i of a new grid is given by the direct inspection of the values corresponding to the old grid cells that intersect c_i. The methods in this class (e.g. the *nearest neighbor*, [9], *area weighted mean*, [57], *and kriging methods*, [5]) approximate the discrete raster function. In [17], the authors develop a rescaling method also applicable to the transformation of grid configuration (from rectangular to

triangular or hexagonal). The method is based on sampling points on the original grid located around the point in the center of a pixel of the rescaled grid. The kriging methods are well suited for irregular sample points and they are not effective on regular and dense grids. Moreover, they require a set of information concerning the correlation functions. Such information must be known in advance or can be inferred by a proper process from the existing data (see also [35, 10]). The multi-stage class methods [9, 32] assume the existence of one or more intermediate (everywhere defined) functions from which the cell values in the new grid are sampled. In this article, we propose a two stage method similar to one widely used in image resampling, [9, 32]. The basic assumption is that the raster values represent the point values of an everywhere defined function that models a certain physical property. In most cases, the function is not analytically known and the raster values are calculated from the values of this function on a set of irregular spatially distributed points. The idea of constructing an intermediate stage is that an extension function is closer than the raster to the model function. Using this method, the hexagonal raster tends to approximate the model function rather than its raster representation. The construction of the intermediate function is essentially based on 2D bicubic interpolation. The bicubic interpolating polynomial is widely used in geomorphology, hydrology, image processing, computer graphics, [37]. It is known that the way one chooses the interpolating polynomial is not unique, but it strongly depends on the specifics of the data one has to interpolate.

1.2 Applications of hexagonal raster

As an application for this hexagonal raster, we propose an iterative cellular automaton based method to model the drainage network of a given landscape. Such channel networks are of interest in domains as hydrology, geomorphology, ecology etc.

The water flow on hill slopes is a complex phenomenon that needs a lot of information concerning the physical properties about the soils and plant cover of the terrain. Focusing only on water path, one ignores all these details and builds simplified models based only on the terrain topography. In this approach, the water is viewed as a thin film flowing (like rolling balls) from a cell to its adjacent neighbors. There are at least two reasons to use hexagonal instead of rectangular raster: the cell adjacency and the local symmetry of the hexagonal structure. For the square grid case, each cell has

four adjacent neighbors with which shares a face and other four with which shares a corner (all these eight neighbors forming the well known Moore neighborhood[1]), and thus, some kind of anisotropy is induced by this type of structure. In contrast, the adjacent cells in a hexagonal raster are of the same type, all six neighbors sharing an edge with the central cell and being at the same distance from its center; this implies no ambiguity in defining the first order neighborhood of a given cell. Such kind of adjacency and the superior symmetry of the cells make the hexagonal raster more suitable to model water flow, erosion, population migration etc. By example, it was observed, [8], that flow direction vectors are better preserved for hexagonal instead of square tilled grids when one moves from one scale to another. Moreover, concerning the properties of symmetry, [14] showed that the mean values obtained using square lattice-gas cellular automata models do not obey the Navier-Stokes equations (although the model conserves mass and momentum) due to the lack of enough symmetry, whereas hexagonal symmetry is sufficient [60]. This emphasizes the local group of symmetries can have major implications when passing from local to global level.

For regular square networks, there are many methods [41, 43, 46, 52] to extract the drainage network. All these methods assume a flow routing algorithm and a criterion for establishing if a cell belongs to or doesn't belong to the discharge network. The common drawbacks of such approaches are the drainage pattern's dependence on the grid resolution [42], the problems of pits (there is no downstream flow from a cell pit) and flat regions (the flow direction cannot reliably be obtained from the neighboring cells [25, 49]) We propose here a hybrid method which combines a hexagonal flow routing scheme with cellular automaton. Due to their simplicity, reduced numerical effort, and fast computational speed, cellular automata are currently frequently used for numerical simulation of natural phenomena, see [4, 6, 13, 12, 38, 47, 58] to cite a few. Regular cellulars based on squares are directly compatible with GIS rasters and therefore, they are almost always met when modelling with such input data. However, there are situations when simulations by cellular automata on hexagonal grids are more suitable than the ones on rectangular grids, [2, 7, 13, 44].

In Section 2 we present a general overview of DP method we are proposing

[1]There are situations when models with Moore type neighbors are suitable, e.g. the discrete approximation of PDEs. On the other hand, there are physical situations where the boundary length between cells and a better network symmetry play an important role, and therefore this type of neighborhood is not anymore adequate.

in this article and we argue in its favor. After introducing some necessary notations, we describe in Section 3 the Essentially Non-Oscillating (ENO) and Outlier Filtering (OF) algorithms used to build the 1D interpolant. We then present the construction of the 2D intermediate function which uses the above 1D interpolant. The last part of this section is devoted to the process of DP where we first describe the construction of a hexagonal network and then present the numerical GIS data conversion of this network. The algorithms accompanying the DP method are detailed in A. Section 4 is dedicated to the validation process of DP method and is divided into two parts. We analyze the errors of DP using a theoretical and then a practical dataset consisting of terrain elevation data provided by GIS rasters. The second part of this section describes a routing method built for the hexagonal raster. The routing method is based on a simplified model of hexagonal cellular automaton for water flow and is applied to real GIS data of some zones from the Romanian territory. The conclusions, perspectives and observations are presented in the last section of this article.

2 Method

Usually, when dealing with exact interpolation by smooth functions, there is a class of data that introduces spurious oscillations (Gibbs phenomenon, [33]). In order to eliminate this phenomenon, we propose an ENO method. ENO provides an exact and continuous interpolant for a given 1D reticulated function, and tries to minimize (in some sense described in Section 3.1) the oscillations produced by interpolation on the discontinuity zones of the reticulated function.

Another undesirable complication is related to the possible presence of the data outliers. In this case, before using any interpolation method, one usually tries to filter these outliers. In this article, we propose a direct interpolation OF method. OF eliminates the eventually rare abnormal data of a reticulated function, but does not always provide an exact and continuous interpolant.

The transition from the square to a hexagonal raster data is accomplished in four steps. First, starting from the square raster, one defines the 2D reticulated function on the set of all square centers; its value at any such center is equal to the raster datum of the square containing that center. Using this function, one then constructs the intermediate (extension) function which will be defined at any point from the square raster domain. Next, one

defines the hexagonal cellular network, and finally constructs the hexagonal raster: the value of the hexagonal raster function on any cell will be given by the value of the intermediate function at its center.

3 2D Bi-cubic Extension

The function extension problem is too wide a field of mathematics to be tackled in a single paper, so we restrict ourselves to a narrow subject that can be formulated as follows. Let $\mathcal{D}$ be a rectangular domain in $\mathbb{R}^2$ and $\mathcal{N}$ a finite set of points (x_i, y_j) in $\mathcal{D}$. A reticulated function is defined by

$$g : \mathcal{N} \to \mathbb{R},\ \mathcal{N} = \bigcup_{i,j} \{(x_i, y_j)\},\ g(x_i, y_j) = g_{i,j}. \tag{1}$$

If one thinks of the reticulated function g as a restriction to $\mathcal{N}$ of a function G defined on the entire domain $\mathcal{D}$, then it makes sense, when given g, to ask about the values of G at a point outside of $\mathcal{N}$ (see [51] for an interesting discussion concerning the meaningfulness of spatio-temporal interpolation of the discrete data).

By extension of the reticulated function (1) one means a numerical scheme to estimate the value of G at any point $(x, y) \in \mathcal{D}$. A bi-cubic extension of the reticulated function (1) is a function defined on the entire domain $\mathcal{D}$ that is a piecewise bi-cubic polynomial function $\widetilde{g} \in \pi_{3,3}$, where $\pi_{3,3}$ designates the set of all polynomials of degree three in each of the two variables x and y

$$\widetilde{g} : \mathcal{D} \to \mathbb{R},\ \mathcal{D} = \bigcup_a \omega_a,\ \widetilde{g}(x, y)\Big|_{\omega_a} \in \pi_{3,3}, \tag{2}$$

with ω_a the elements of a cell partition of $\mathcal{D}$.

The problem of the bi-cubic extension can be formulated as follows: *given a reticulated function* (1)*, define the extension* (2) *that approximates the model function* $G : \mathcal{D} \to \mathbb{R}$.

In what follows, we propose two methods to define a bi-cubic extension, both of them assuming a 1D extension method. The 2D extension method is obtained by successively applying the 1D method once along the Ox and then along the Oy directions.

To define the 1D algorithm, we need to introduce some notations. Let $\Xi := \{\xi_i\}_{i=\overline{1,N}}$ be a set of 1D consecutive knots inside a generic interval $[\alpha, \beta]$,

with $\alpha \leq \xi_1 < \ldots < \xi_N \leq \beta$, and $\{f_i\}_{i=\overline{1,N}}$ the values of some reticulated function f at these points. There are different formula to write the unique cubic polynomial that equals the values f_{i_k} at four distinct knots $\{\xi_{i_k}\}_{k=\overline{1,4}}$. The Newton's form of the Lagrange interpolation polynomial reads as [45]

$$\begin{aligned}\mathcal{P}_{(i_1,i_2)}^{f;(i_3,i_4)}(\xi) \; &:= f(\xi_{i_1}) + (\xi - \xi_{i_1})[\xi_{i_1};\xi_{i_2}]f + \\ &+(\xi - \xi_{i_1})(\xi - \xi_{i_2})\Big([\xi_{i_1};\xi_{i_2};\xi_{i_3}]f + (\xi - \xi_{i_3})[\xi_{i_1};\xi_{i_2};\xi_{i_3};\xi_{i_4}]f)\Big),\end{aligned} \tag{3}$$

where $[\cdot;\cdot]$, $[\cdot;\cdot;\cdot]$ and $[\cdot;\cdot;\cdot;\cdot]$ represent the divided difference operators of order one, two and three, respectively. The divided difference operator is recursively defined as

$$\begin{aligned}[\xi_{i_1};\xi_{i_2}]\, f &= \frac{f_{i_2} - f_{i_1}}{\xi_{i_2} - \xi_{i_1}}, \\ \left[\xi_{i_1};\ldots;\xi_{i_{n+1}}\right] f &= \frac{\left[\xi_{i_2};\ldots;\xi_{i_{n+1}}\right] f - \left[\xi_{i_1};\ldots;\xi_{i_n}\right] f}{\xi_{i_{n+1}} - \xi_{i_1}},\end{aligned}$$

where the knots ξ_{i_j} are all different from each other.

For any $k = \overline{1, N-1}$, we denote by I_k^ξ the open interval

$$I_k^\xi := (\xi_k, \xi_{k+1}), \tag{4}$$

and by S_k^ξ the set of up to six consecutive knots

$$S_k^\xi := \{\xi_{k-2}, \xi_{k-1}, \xi_k, \xi_{k+1}, \xi_{k+2}, \xi_{k+3}\} \cap \Xi. \tag{5}$$

S_k^ξ defines a neighborhood of knots that can influence the values of the extension function of f on the interval I_k^ξ.

3.1 1D Essentially Non-Oscillating Extension (ENO) Algorithm

The ENO type extension operator was first introduced in the context of numerical approximation of hyperbolic system of partial differential equations, [21, 22], in order to reduce the Gibbs oscillations that appear in the reconstruction of the shock wave solution. In [26], the ENO algorithm (6) was used to perform the multiresolution analysis of a 1D reticulated function defined on a bounded interval. For each I_k^ξ, the method defines an interpolant

$\mathcal{P}^{f;(i_3,i_4)}_{(i_1,i_2)}(\xi)$ associated to the four distinct consecutive knots $\xi_{i_1}, \xi_{i_2}, \xi_{i_3}, \xi_{i_4}$ from S^{ξ}_k, by setting $i_1 := k$, $i_2 := k+1$, and choosing i_3, i_4 such that $\mathcal{P}^{f;(i_3,i_4)}_{(k,k+1)}(\xi)$ has, in some sense, the smallest oscillation on the interval $\bar{I}^{\xi}_k$.

Specifically, we compare the above cubic polynomials associated to the interval $\bar{I}^{\xi}_k$ with the linear interpolant corresponding to the same interval because linear interpolation is exact and it does not have oscillations. We want to select the "nearest" cubic polynomial with respect to the linear interpolant. In order to achieve this, we choose as a measure of oscillation, the $\mathbb{L}^2(I_k)$ distance[2] between $\mathcal{P}^{f;(i_3,i_4)}_{(k,k+1)}$ and the linear interpolant $\mathcal{Q}^f_k(\xi) := f(\xi_k) + (\xi - \xi_k)[\xi_k; \xi_{k+1}]f$. Therefore, using the simplifying notations $\mathcal{P}^f_{-1} := \mathcal{P}^{f;(k-2,k-1)}_{(k,k+1)}$, $\mathcal{P}^f_0 := \mathcal{P}^{f;(k-1,k+2)}_{(k,k+1)}$, $\mathcal{P}^f_1 := \mathcal{P}^{f;(k+2,k+3)}_{(k,k+1)}$, the 1D ENO algorithm can now be sketched as

---

$$\begin{aligned} &\text{Find } a \text{ s.t. } a = \underset{b\in\{-1,0,1\}}{\arg\min} \left\| \mathcal{P}^f_b - \mathcal{Q}^f_k \right\|_{\mathbb{L}^2(I^{\xi}_k)}. \\ &\text{If } a \text{ is not unique, then choose } a := 0. \\ &\text{Set } \widetilde{f}(\xi) := \mathcal{P}^f_a(\xi), \quad \forall \xi \in \bar{I}^{\xi}_k := [\xi_k, \xi_{k+1}]. \end{aligned} \tag{6}$$

3.2 1D Outlier Filtering Extension (OF) Algorithm

As in the ENO algorithm, for each I^{ξ}_k, one determines the polynomial $\mathcal{P}^{f;(i_3,i_4)}_{(i_1,i_2)}$ such that the quantity

$$\left\| \frac{\mathrm{d}^2}{\mathrm{d}\xi^2} \mathcal{P}^{f;(i_3,i_4)}_{(i_1,i_2)} \right\|_{\mathbb{L}^2(I^{\xi}_k)},$$

is minimized. Unlike the ENO method, the OF method generally defines a non-continuous extension function (possible discontinuities at the knots ξ_j). The advantage of the method is that the extension function does not take into account the "bad" points (outliers), points where the function (its value) strongly deviates from a "regular behavior".

Both the ENO and OF methods have the property of recovering polynomial functions of degree up to three, i.e. if the reticulated function f is

[2]We choose the $\mathbb{L}^2$ distance for attenuating interpolation oscillations because the resulting formulas are quite simple and easily to introduce in the code. One can use $\mathbb{L}^1$ or some $\mathbb{L}^p$ distance. We have no arguments that one of them is the best.

generated by a third degree polynomial $P(\xi)$ then $\widetilde{f}(\xi) \equiv P(\xi)$, for any ξ.

The 1D OF algorithm can now be sketched as:

$$\begin{array}{l} \text{Find } i_1, i_2, i_3, i_4 \text{ s.t.} \\ \{\xi_{i_l}\}_{l=\overline{1,4}} = \underset{\xi_l, \xi_m, \xi_p, \xi_q \in S_k^{\xi}}{\arg\min} \left|\left| \dfrac{\mathrm{d}^2}{\mathrm{d}\xi^2} \mathcal{P}_{(l,m)}^{f;(p,q)} \right|\right|_{\mathbb{L}^2(I_k^{\xi})}. \\ \text{Set } \widetilde{f}(\xi) := \mathcal{P}_{(i_1,i_2)}^{f;(i_3,i_4)}(\xi) \quad \forall \xi \in I_k^{\xi}. \end{array} \tag{7}$$

As previously mentioned, choose the value of $\widetilde{f}$ at any knot ξ_j to be one of the lateral limits or their average.

Two illustrative examples of 1D ENO and OF methods can be found in Figures 2 and 3.

3.3 2D Extension Scheme

Let g be a 2D reticulated function of the form (1). As the 1D case, one introduces $I_k^x := (x_k, x_{k+1})$, $I_l^y := (y_l, y_{l+1})$ and the corresponding sets S_k^x, S_l^y, respectively, of form (5). Denote also by $\omega_{k,l}$ the domain

$$\omega_{k,l} = I_k^x \times I_l^y.$$

Let $(x, y) \in \omega_{k,l}$. The key idea is to define an extension function as a cross combination of 1D algorithms. At first, for any y_m, one can define an extension function $\widetilde{f}(x, y_m)$ by using a 1D method with respect to an x variable. The restriction $\widetilde{f}_k(x, y_m)$ of this function to the interval I_k^x can be written as

$$\begin{array}{rl} \widetilde{f}_k(x, y_m) := & g(x_{i_1}^m, y_m) + (x - x_{i_1}^m)[x_{i_1}^m; x_{i_2}^m] g(\cdot, y_m) + \\ & + (x - x_{i_1}^m)(x - x_{i_2}^m)[x_{i_1}^m; x_{i_2}^m; x_{i_3}^m] g(\cdot, y_m) + \\ & + (x - x_{i_1}^m)(x - x_{i_2}^m)(x - x_{i_3}^m)[x_{i_1}^m; x_{i_2}^m; x_{i_3}^m; x_{i_4}^m] g(\cdot, y_m), \end{array}$$

where the knots $\{x_{i_l}^m\}_{l=\overline{1,4}}$ belong to S_k^x and they are given by the 1D method. By $[x_{i_1}^m; \ldots; x_{i_n}^m] g(\cdot, y_m)$ one means the divided difference operator that acts on the reticulated function $f := g(\cdot, y_m)$ and the knots $\{x_{i_j}^m\}_{j=\overline{1,n}}$.

Then, keeping x and having $\widetilde{f}_k(x, y_m)$ for each $y_m \in S_l^y$, and using again a 1D method, this time with respect to y variable, one sets the value of the

extension function $\widetilde{g}$ as

$$\begin{aligned}\widetilde{g}(x,y) := \quad & \widetilde{f}_k(x,y_{i_1}) + (y-y_{i_1})[y_{i_1};y_{i_2}]\widetilde{f}_k(x,\cdot)+ \\ & +(y-y_{i_1})(y-y_{i_2})[y_{i_1};y_{i_2};y_{i_3}]\widetilde{f}_k(x,\cdot)+ \\ & +(y-y_{i_1})(y-y_{i_2})(y-y_{i_3})[y_{i_1};y_{i_2};y_{i_3};y_{i_4}]\widetilde{f}_k(x,\cdot).\end{aligned}$$

One notes that the extension function $\widetilde{g}(x,y)$ can have some discontinuous line $x=\overline{x}$ even inside of a rectangle $\omega_{k,l}$.

See A for comments on the mathematical properties on the extension functions $\widetilde{g}$.

When compared to the filter reconstruction, this nonlinear method is time consuming. Though, since it is used only once in the beginning when we transfer data from the GIS raster to the hexagonal raster, we can benefit by applying this method since the Gibbs phenomenon is no longer present. This can be important when big jumps appear in the data (for example, the landscape elevation in rough terrain).

3.4 Data Porting

In this section, we present a method to construct the data set on a regular hexagonal raster starting from a raster data set used by GIS. The data transformation from a GIS raster to a hexagonal raster involves two main steps: the hexagonal tessellation of the domain on which the GIS raster is defined and the method of assigning values to the hexagonal raster cells. First, we present the geometry of a hexagonal raster including the number of cells, their size and relative positions. Then, we present the method of data transfer for real valued functions.

3.4.1 Hexagonal raster

The hexagonal raster differs from a GIS raster by the cell type used to tessellate the area of interest, with regular hexagons instead of square cells being used for this tessellation.

The data set can be structured as rows and columns such that each row has an equal number of cells. Let M and N be the number of rows and columns, respectively, and let r be the radius of the circumscribed circle of the regular hexagon. From a computational point of view, besides the "parameters" M, N and r, one needs to know the position of the hexagon centers with respect to a coordinate system.

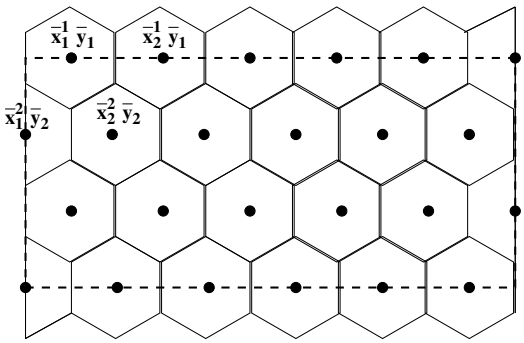

Figure 1: An example of hexagonal tessellation.

Let $\mathcal{D}$ be a rectangular domain whose sides are parallel to the xOy coordinate system axes. A tessellation of $\mathcal{D}$ (Figure 1) can be defined as follows. For any $i = \overline{1, N}$ and $j = \overline{1, M}$, let $x_{i,j}^h$ and $y_{i,j}^h$ be the coordinates of the center of the hexagonal cell $h_{i,j}$. We denote by $\widetilde{x}_0$ and $\widetilde{y}_0$ the coordinates of the upper left cell center in the tessellation, and define the knots $(\widetilde{x}_i^j, \widetilde{y}_j)$ by

$$\begin{aligned}\widetilde{x}_i^j &= \widetilde{x}_0 + (i-1)r\sqrt{3} - (j-1)\%2\frac{r\sqrt{3}}{2},\\ \widetilde{y}_j &= \widetilde{y}_0 + 3(j-1)\frac{r}{2},\end{aligned}$$

where $a\%2$ represents the remainder of the division of a by 2. One now sets

$$x_{i,j}^h := \widetilde{x}_i^j, \quad y_{i,j}^h := \widetilde{y}_j.$$

3.4.2 Porting real numerical data from a rectangular to hexagonal raster

The method of a rectangular raster data storage consists of: a rectangular domain $\mathcal{D}$, a function G defined on $\mathcal{D}$, a tessellation of $\mathcal{D}$ with regular rectangular cells $c_{i,j}$, and an approximation g^r of the function G by constant values $g_{i,j}^r$ on $c_{i,j}$,

$$g^r : \mathcal{D} \to \mathbb{R},\ \mathcal{D} = \bigcup_{i,j} c_{i,j},\ g^r(x,y)\Big|_{c_{i,j}} = g_{i,j}^r. \tag{8}$$

The basic idea is to use an intermediate extension function in the conversion procedure. Let (x_i, y_j) be the center of the cell $c_{i,j}$, $\mathcal{N}$ the set of all these centers and let g be the reticulated function defined by

$$g : \mathcal{N} \to \mathbb{R},\ g(x_i, y_j) = g^r_{i,j}.$$

Using a 2D extension algorithm, one can construct the extension function

$$\widetilde{g} : \widetilde{\mathcal{D}} \to \mathbb{R},$$

of g and then define

$$g^h : \widetilde{\mathcal{D}} \to \mathbb{R},\ g^h(x, y)\Big|_{h_{i,j}} = \widetilde{g}(x^h_{i,j}, y^h_{i,j}),$$

where $h_{i,j}$ denotes the hexagonal cell of center $(x^h_{i,j}, y^h_{i,j})$, and $\widetilde{\mathcal{D}} := \bigcup_{i,j} h_{i,j}$.

4 Validation and Numerical Applications

The main steps of DP method introduced in Section 3.4.2 can be summarized by the following chain

$$g^r \to \widetilde{g} \to g^h.$$

The accuracy of g^h can be analyzed with respect to the raster function g^r, and with respect to the function, say G, which models the physical property represented by the raster data. From an application point of view, the most important is the accuracy of g^h with respect to G. One can estimate the errors between g^h and G in some simple cases (e.g. when g^r is directly obtained from G using some mathematical operations), but not in general because it depends on the way g^r is produced. We now proceed to analyze the accuracy of our DP method by using some theoretical examples as well as a case of digital terrain model. We begin this section illustrating how the extension methods work for the 1D case. Figure 2 presents four graphics: the model function G, the raster g^r, the reticulated function, and the extension function $\widetilde{g}$ obtained by ENO method. The OF method (when some outliers are present) is exemplified in Figure 3.

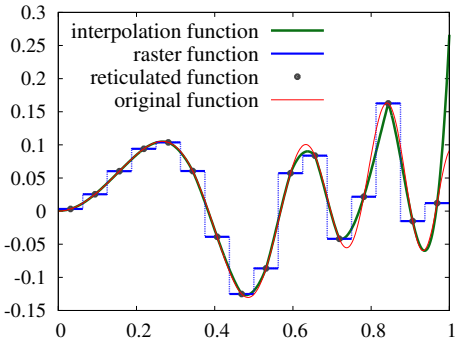

Figure 2: Illustration of the 1D ENO algorithm. One can remark that the interpolated function is "closer" to the original function (some smooth function which plays here the role of the function G) than the raster function. Note that *it is generally better to approximate the original function by the interpolation rather than the raster function.*

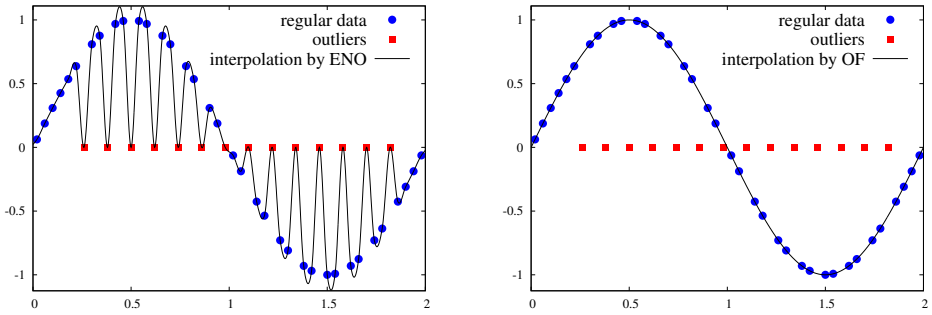

Figure 3: ENO vs OF in the presence of outliers. Starting from $\sin(\pi x)$ we have generated a reticulated function where a part of the data have been "corrupted" with the value 0. The above figures represent the reticulated function (dots) and extension function (continuous line) obtained by the interpolation methods ENO (on left) and OF (on right). One can observe that the first method is not appropriate for this kind of data, it does not recognize the outliers, the second method makes a good attempt at this. This behavior of ENO is typical of all exactly interpolating methods.

4.1 Errors in data porting

There are four major sources of errors affecting data in a hexagonal raster obtained by DP (from a rectangular raster) as a quantitative model of some physical property:

• the error between the values of the physical property and the mathematical function G which models this property (the modelling error);

• the error between the function g^r provided by the GIS raster data and G;

• the error between g^r and its interpolant $\widetilde{g}$;

• the error introduced by the discretization of $\widetilde{g}$ on the hexagonal cells represented by g^h.

As our entry data in DP are raster data, we can only control the last two components of the error. The better control of these errors gives a better representation of G by g^h. We first investigate the accuracy of g^h with respect to G by considering two theoretical examples where we know the analytic form of G, as well as the way g^r is obtained from G. We then analyze the errors for some Digital Elevation Model (DEM).

4.1.1 Theoretical case study

Let *real physical data* be modeled by the (Runge type) function of parameter a,

$$G(x, y; a) = \frac{a}{(1 + x^2)(1 + y^2)}, \tag{9}$$

and let g^r be a square raster approximation of it. In our example, we choose a domain $\mathcal{D} = [-20, 20] \times [-20, 20]$ and define two raster data with regular partitions. The first one, denoted by SR1, has 41×41 cells, and the second one, denoted by SR2, has 201×201 cells. For each of these two partitions, let g^r be a square raster approximation of G (on any square cell g^r equals the value of G at its center).

Now, given the raster data g^r, one can build a hexagonal raster following the method described in the previous section. To emphasize the approximation behavior of our method, we construct several hexagonal rasters, each one being defined by the number of the cells considered along the Ox direction. The number of cell rows along the Oy direction results from the requirement to cover the domain $\mathcal{D}$. We choose five cases corresponding to $50, 100, 200, 300$ and 600 horizontal cells. As an error measure, we consider

the $\mathbb{L}^1$-distance between two functions. Thus, define

$$\varepsilon_{hr} := \frac{1}{\gamma}\int_{\Omega}\left|g^r - g^h\right|\mathrm{d}\xi, \quad \varepsilon_{ha} := \frac{1}{\gamma}\int_{\Omega}\left|G - g^h\right|\mathrm{d}\xi, \quad \varepsilon_{ra} := \frac{1}{\gamma}\int_{\Omega}\left|G - g^r\right|\mathrm{d}\xi,$$

where $\Omega := \mathcal{D}\cap\widetilde{\mathcal{D}}$, and $\gamma := \int_{\Omega}|g^r|\mathrm{d}\xi$. The numerical results for these errors are graphically illustrated in Figure 4, for parameter $a = 1$ in G.

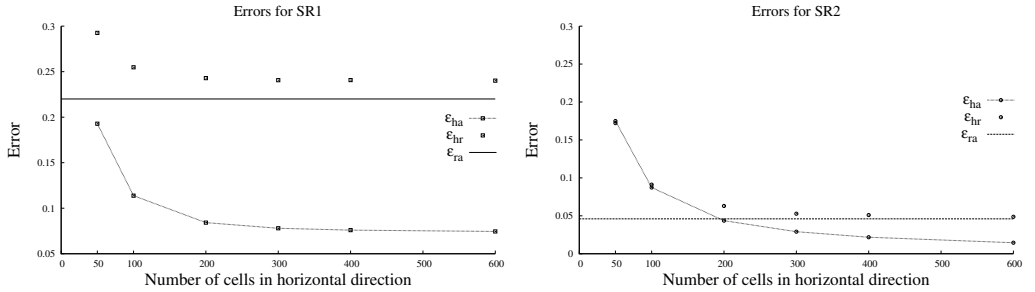

Figure 4: The behavior of the errors ε_{hr} and ε_{ha} as function of the hexagonal raster dimension.

One should remark that, in general:

a) for a given GIS raster function g^r, the error ε_{hr} does not go to 0 as the hexagonal cell radius goes to 0;

b) g^h tends to approximate the mathematical function G rather than the approximation g^r of G, $\varepsilon_{hr} > \varepsilon_{ha}$;

c) if the number of cells is high enough, then g^h is a better approximation of the mathematical model expressed by function G than its first approximation g^r;

d) a better approximation of G by g^r improves the quality of the entire approximation scheme.

This behavior lies in the fact that g^h approximates $\widetilde{g}$, while $\widetilde{g}$ tries to recover the function G (and this holds if G satisfies some regularity properties).

In the next theoretical example, we analyze the fidelity of representing G with $\widetilde{g}$. By fidelity, we mean a characteristic of the method of not introducing spurious artifacts (bumps, pits, oscillations etc.) which are not supported by the raster data. Here, we compare ENO to filter reconstruction method (Catmull-Rom cubic spline (CRS), [9]), well known and often used due to their efficiency in constructing smooth functions from discrete data. We mention that both methods use cubic polynomials and have the same accuracy.

Using a 10×10 raster covering the rectangular domain $[-14, 14] \times [-14, 14]$ generated with the Runge type function $G(x, y; 10)$ from (9), we try to reconstruct the original function by ENO and CRS methods. Figure 5 presents a comparison for such a case between these two methods. We have specifically chosen such a low resolution raster in order to highlight that a scarcity of the data (as in some environmental applications) may lead to poor results when the chosen extrapolation method is inappropriate. Although the CRS reconstructed $\widetilde{g}_{CRS}$ is smoother (also the $\mathbb{L}^1$ error is a slightly better) than the one of ENO, we remark that $\widetilde{g}_{CRS}$ exhibits unpleasant artifacts. We mention that, if a higher resolution raster is chosen, then both methods give very good results.

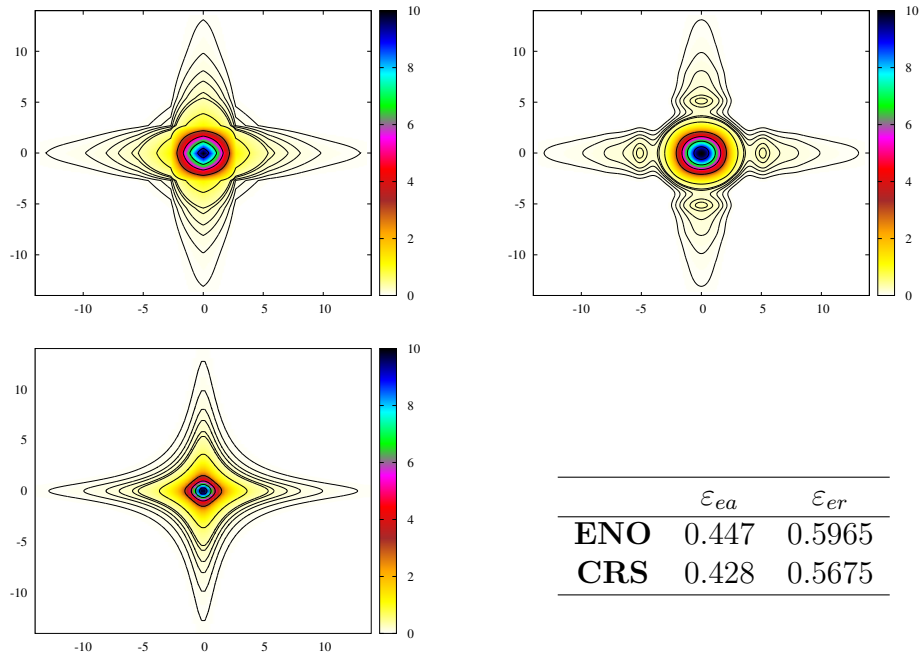

	ε_{ea}	ε_{er}
ENO	0.447	0.5965
CRS	0.428	0.5675

Figure 5: Comparison between 2D ENO and CRS. The level curves of these two extension functions are drawn in the upper left and right pictures for ENO and CRS, respectively. The level curves of G are represented in the lower left image. The relative $\mathbb{L}^1$ errors of the extension functions, defined as $\varepsilon_{ea} = ||\widetilde{g} - G(x, y; 10)||/||g^r||$, $\varepsilon_{er} = ||\widetilde{g} - g^r||/||g^r||$ are given in the table.

4.1.2 Case study with GIS data

In this section, we use GIS data from Ampoi's Valley with large cells (100 m cell size) and from Paul's Valley - a subdomain in Ampoi's basin - with much smaller cells (10 m cell size).

First, we analyze the behavior of our DP method with respect to the input data density, using the GIS from Paul's Valley. This represents the basis raster we refer in the next example. One associates a reticulated function g to this raster as in Section 3.4.2, i.e.

$$g : \mathcal{N} \to \mathbb{R},\ \mathcal{N} = \bigcup_{i,j} \{(x_i, y_j)\},\ g(x_i, y_j) = g^r_{i,j},$$

where (x_i, y_j) and $g^r_{i,j}$ are the centers and GIS values on the squares, respectively. Starting from this basis raster, we construct several rasters by randomly eliminating part of the data (replacing them with NODATA_VALUE), this process being achieved with some restrictions described in B. Then we associate a reticulated function $g_{(\alpha)}$ to such a raster α,

$$g_{(\alpha)} : \mathcal{N}_{(\alpha)} \to \mathbb{R},\ \mathcal{N}_{(\alpha)} \subset \mathcal{N},\ g_{(\alpha)} = g \text{ on } \mathcal{N}_{(\alpha)},$$

where $\mathcal{N}_{(\alpha)}$ is the set of the remaining square centers.

To test the capability of ENO method to recover the missing data, we apply it to $g_{(\alpha)}$ for constructing the extension function $\widetilde{g}_{(\alpha)}$ by means of which we can calculate the values at the points from $\mathcal{N} \setminus \mathcal{N}_{(\alpha)}$. Now, one has to compare these values with the corresponding ones from the basis raster. For this purpose, we use two different measures:

1. the root-mean-square error[3] (RMSE)

$$RMSE = \sqrt{\frac{1}{\nu} \sum_{i,j} \left(g^r_{i,j} - \widetilde{g}_{(\alpha)}(x_i, y_j)\right)^2},$$

   where[4] $\nu = \#\left(\mathcal{N} \setminus \mathcal{N}_{(\alpha)}\right)$;

2. the infinity norm of $g - \widetilde{g}_{(\alpha)}$ on $\mathcal{N}$

$$||g - \widetilde{g}_{(\alpha)}||_\infty = \max_{i,j} |g^r_{i,j} - \widetilde{g}_{(\alpha)}(x_i, y_j)|.$$

[3]Since ENO is an exact interpolation method, the expressions $g^r_{i,j} - \widetilde{g}_{(\alpha)}(x_i, y_j)$ obviously vanish for $(x_i, y_j) \in \mathcal{N}_{(\alpha)}$.

[4]The notation $\#A$ for some set A stands for the cardinal of A.

Then, the accuracy of DP is analyzed by comparing the basis hexagonal raster g^h generated by $\widetilde{g}$ with the hexagonal rasters $g^h_{(\alpha)}$ generated by $\widetilde{g}_{(\alpha)}$. These measures are calculated for different cases α and presented in Table 2.

Table 2: This table presents the errors between a basis square raster and different test square rasters (α) by means of RMSE and $\|\cdot\|_\infty$ in columns 3 and 4, respectively. The errors between the basis hexagonal raster (built from the basis square raster using ENO) and the test hexagonal rasters (built from test square rasters using again ENO) are given in columns 5 and 6. The basis square raster with cell size of 10 m contains 361×561 GIS data from Romanian Paul's Valley, while the hexagonal rasters are based on cells of 10.418 m size.

		Square Rasters		Hexagonal Rasters	
α	$\#\mathcal{N}_{(\alpha)}/\#\mathcal{N}$	RMSE	$\|\|\cdot\|\|_\infty$	RMSE	$\|\|\cdot\|\|_\infty$
1	0.25	0.097	2.33	0.076	2.230
2	0.21	0.106	2.50	0.086	2.500
3	0.17	0.121	3.40	0.102	3.420
4	0.14	0.123	2.66	0.109	1.957
5	0.12	0.137	3.73	0.122	3.370

As we have commented in the beginning of Section 4, it is almost impossible to measure the error between the raster g^h and the physical quantity G modeled by it (we do not know this function). However, we can perform an analysis of the accuracy when we have two different rasters of the same area, one at a low and the other at high resolutions. It is assumed that the high resolution raster is a good approximation of G. In such case, we generate the extension function from the low resolution raster, and then we compare it to the high resolution raster function. Following this strategy, we therefore perform a qualitative and then a quantitative analysis.

Figure 6 presents pictures of the same portion of Paul's Valley terrain obtained from different raster data. In this figure, as well as in Figures 9 and 10, the color codes correspond to altitudes which are measured in meters. The left and the middle images are generated by rectangular rasters of 100 and 10 m cell size, respectively. The right image "pictures" the accuracy of our DP method with respect to the "real" function G behind the data rasters and it is build on a hexagonal raster (of 5.7735 m cell size) obtained from the low resolution rectangular raster corresponding to the left image. The resemblance of this figure to the one in the middle which is built from a much

denser GIS raster represents an argument that our DP is able to recover the "real" function G. This result is similar to the theoretical cases previously studied. Moreover, this resemblance can be also verified with the airplane photo from Figure 10.

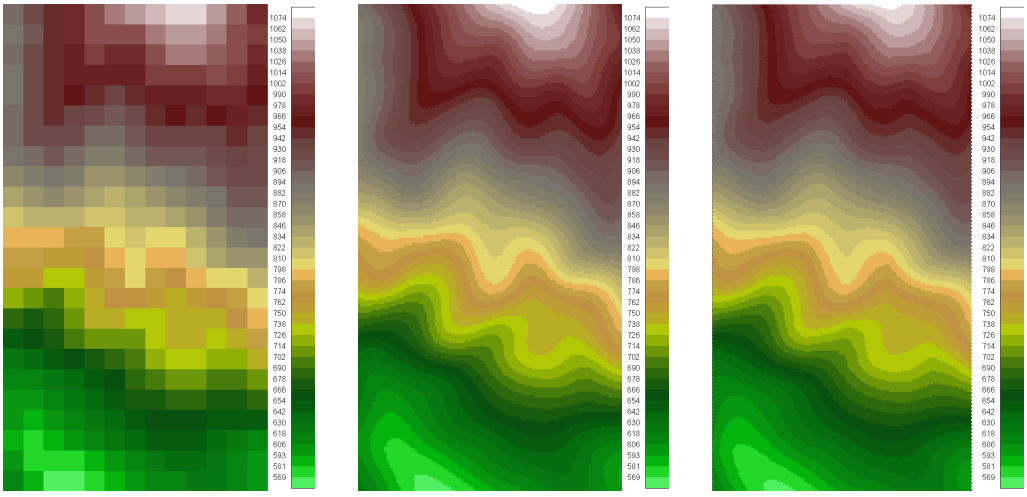

Figure 6: Relief from Romanian Paul's Valley. All the figures represents the same zone from Romanian Paul's Valley and are obtained as follows: the left one from a 13×24 GIS raster data with square cells of 100 m size, the middle one from a 130×240 GIS raster data with square cells of 10 m size. The figure on the right is obtained on a hexagonal raster (of 5.7735 m cell size) applying our ENO method to the same data input as for the first figure.

The quantitative results of our analysis are summarized in Table 3. One

Table 3: Error analysis for the case study with GIS data. This table contains the relative errors of the extension functions provided by ENO, CRS, and Id (the extension function of Id is identical to the raster function). The analysis is performed using the same two GIS rasters (one of high (H) and the other one of low (L) resolution) as those in Figure 6. $\varepsilon_L^L = ||\widetilde{g}_L - g_L^r||/||g_L^r||$, $\varepsilon_H^L = ||\widetilde{g}_L - g_H^r||/||g_H^r||$, $\varepsilon_H^H = ||\widetilde{g}_H - g_H^r||/||g_H^r||$, where the norms $||\cdot||$ are in $\mathbb{L}^1$. The extension functions $\widetilde{g}_L$, $\widetilde{g}_H$ are generated by the low, and high resolution raster functions g_L^r and g_H^r, respectively.

	ε_L^L	ε_H^L	ε_H^H
ENO	0.0076	0.0033	0.00078
CRS	0.0075	0.0033	0.00078
Id	0.0000	0.0081	0.00000

should remark that:

a) for ENO and CRS, the extension function is closer to the high than lower resolution raster function, although the extension function is build from the lower resolution raster function: $\varepsilon_H^L < \varepsilon_L^L$. This explains why the right picture from Figure 6 is more similar to the middle picture than to the left one.

b) the error between the extension and the high resolution raster function is smaller than the error between the high and the low resolution raster functions: $\varepsilon_H^L(ENO), \varepsilon_H^L(CRS) < \varepsilon_H^L(Id)$. This explains why the middle picture from Figure 6 is more similar to the right picture than to the left one.

c) the extension function generated by the high resolution raster is closer than the extension function generated by the low resolution raster to the high resolution raster function: $\varepsilon_H^H < \varepsilon_L^L$. This says that the extension function generated by the high resolution raster is better than the extension function generated by the low resolution raster.

4.2 Water Routing

By water routing one means a method to define the way cells exchange water between one another or the way water flows along the entire cellular. There exists a large body of literature devoted to the subject, see for example [41, 39, 43, 49, 52, 59], but most of the existent schemes are designed for the square cells. However, there are also a few papers (see [6] for example) where hexagonal instead of square cellulars are used and different water routing schemes are presented. Any water routing scheme assumes two kinds of rules: qualitative and quantitative ones. The qualitative rules give us a picture of the water path, while the quantitative rules give us information about the amount of water discharge along the water path. In what follows, using notions as *donor cells*, *receptor cells*, *steepest descent*, and *water velocity of a cell*, we present a method to model the water path.

First, let us introduce the local configuration of a hexagonal cellular. By local configuration one means a central cell with its six adjacent cells defining the neighborhood of this central cell. The sides of the central cell are indexed from 1 to 6 counterclockwise. One denotes by $\mathcal{V}_i$ the neighbors of a cell i. The quantities referring to the central cell are indexed with 0 and those referring to its neighbors are indexed from 1 to 6, see Figure 7.

Steepest descent and water velocity. For each cell i, define its water po-

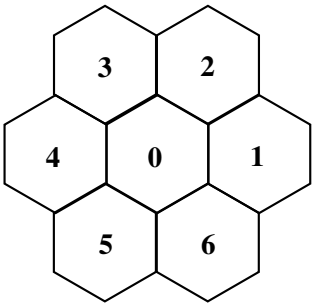

Figure 7: A central cell i (indexed by 0) and its neighbors (indexed from 1 to 6).

tential ψ_i to be

$$\psi_i = h_i + z_i,$$

where h_i denotes the water depth in this cell and z_i stands for the altitude to its soil surface.

We now consider a reference cell i of center (x_0, y_0) and its local configuration with the cells of centers $\{(x_j, y_j)\}_{j=\overline{1,6}}$. One may approximate the tangent plane Π to the surface of the water potential by the best interpolant plane given by the points $\{(x_j, y_j, \psi_j)\}_{j=\overline{0,6}}$. The equation of this plane can be described as

$$z - z_0 = a(x - x_0) + b(y - y_0),$$

where

$$a = \frac{1}{6\sqrt{3}r}, \left(2(\psi_1 - \psi_4) + \psi_2 - \psi_5 + \psi_6 - \psi_3\right),$$
$$b = -\frac{1}{6r}\left(\psi_2 - \psi_5 + \psi_3 - \psi_6\right)$$

and r represents the radius of the circumscribed circle of the hexagon.

The steepest descent of the cell i is defined as the projection of the gravitational force onto its tangent plane Π, and therefore, as a vector in $\mathbb{R}^3$ it is given by

$$\boldsymbol{d} = \left(-a, -b, -(a^2 + b^2)\right)^{\mathrm{T}}.$$

The slope of the cell i is now given by

$$s = \sqrt{\frac{a^2 + b^2}{1 + a^2 + b^2}}, \tag{10}$$

and therefore, the projection versor of the steepest descent onto the xOy plane is given by

$$\boldsymbol{\tau} = \left(-\frac{a}{\sqrt{a^2+b^2}}, -\frac{b}{\sqrt{a^2+b^2}} \right). \tag{11}$$

Receptor/Donor cells. A cell of index j in the neighborhood $\mathcal{V}_i$ of the central cell i is called a *receptor cell* if it satisfies two conditions:

$$\begin{array}{l} \psi_j < \psi_0 \\ \boldsymbol{\tau} \cdot \boldsymbol{n}_{ij} > 0 \end{array} \tag{12}$$

where $\boldsymbol{n}_{ij}$ is the outward unitary normal to the face j of central cell i. The set of all these receptor cells j associated to the cell i will be denoted by J_i^-. If $J_i^- \neq \emptyset$, then i is called a *donor cell*.

Water velocity. The water velocity is calculated using the descent direction (11), the slope (10) and a Manning type empirical law

$$\boldsymbol{w}_i = v(h_i, s_i)\boldsymbol{\tau}_i, \;\; v(s,h) = \frac{h^{2/3} s^{1/2}}{n_M}, \tag{13}$$

where n_M is the Manning coefficient and s the slope of the central cell.

Water flux. The basic assumption on the water flux across the cells is that the water of any cell flows out to the neighboring cells toward which the water velocity of that cell points to, and the water enters a cell only from the neighboring cells whose water velocities point to that cell. This assumption is analogous to the upwind scheme used in hyperbolic system approximation theory [15]. A comparative portrait between Tarboton method on rectangular raster and the above presented method for water flow among cells is illustrated in Figure 8.

Let i be a donor cell. The water lost by the cell i during the time interval $\triangle t$ is given by

$$\triangle t \, l \, h_i \sum_{j \in J_i^-} \boldsymbol{n}_{ij} \cdot \boldsymbol{w}_i, \tag{14}$$

where l is the side of the hexagonal cell. A receptor cell j from the set J_i^- receives a water quantity equal to

$$\triangle t \, l \, h_i \, \boldsymbol{n}_{ij} \cdot \boldsymbol{w}_i. \tag{15}$$

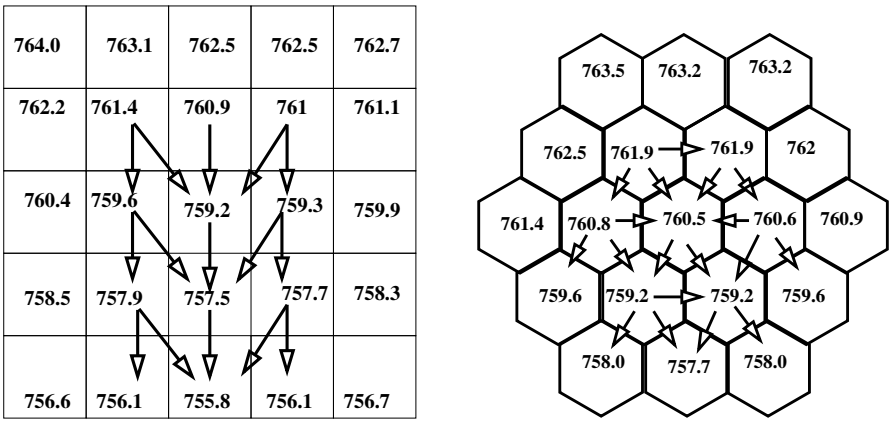

Figure 8: Water flow among cells in rectangular (left side) and hexagonal (right side) rasters using Tarboton and our rules, respectively. Data written inside cells represent altitudes and they come from a small region (the same on the left and on the right) of Romanian Paul Valley. The values of the rectangular raster slightly differ from those of the hexagonal one because they represent two different models of the same terrain surface.

Thus, the water flux trough the boundary of a cell i during the time interval $\triangle t$ is given by

$$\mathcal{F}_i^f = \triangle t\, l \left(-h_i \sum_{j \in J_i^-} \boldsymbol{n}_{ij} \cdot \boldsymbol{w}_i + \sum_{k \in \mathcal{V}_i^+} h_k \boldsymbol{n}_{ki} \cdot \boldsymbol{w}_k \right), \tag{16}$$

where $\mathcal{V}_i^+$ is the set[5] of neighboring cells of i shedding water to this cell.

One can now define the water flow as an iterative process by

$$h_i^{n+1} = h_i^n + \mathcal{F}_i^{f,n}, \tag{17}$$

where $\mathcal{F}_i^{f,n}$ represents the water flux trough the boundary of a cell i during the time interval $\triangle t$ at the n^{th} iteration.

Figure 9 is a snapshot of a water flow modeled using the method described in this section.

Figure 10 contains three images of the same zone cut out from Paul's Valley. The first one is a photo where one can observe the ravines of this region, while the other two are images constructed from GIS data and include

[5] $\mathcal{V}_i^+ = \{ k \in \mathcal{V}_i \mid \exists j \in J_k^- \text{ s.t. } i = M(j,k) \}$, where $M(j,k)$ represents the index of that cell from $\mathcal{V}_k$ sharing with k the common face j.

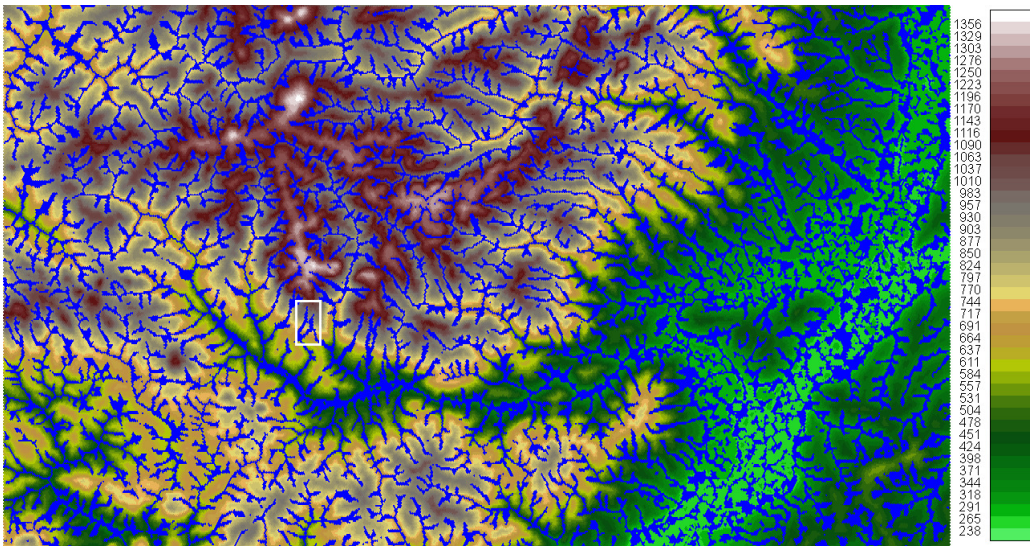

Figure 9: Water accumulation zones in Ampoi's hydrographic basin. Starting from the real elevation GIS raster data (542 columns by 310 rows of cells with 100 m side length) of Ampoi's landscape, we captured the areas of concentrated water flow using a hexagonal cellular automaton. The hexagonal raster (with cell side of 57.735 m) was obtained by porting the GIS data following the method described in Section 3.4. Beginning with a uniform shallow water level for the entire landscape, we processed for a set time interval the water flow across the cells using the law described by (16). The blue area in the figure represents the hexagonal cells where the water layer exceeds the initial level. The white border rectangle inside this figure marks the area from Paul's Valley we have referred in Figures 6 and 10.

the water accumulation zones found in two different ways. It is known that if Tarboton's rules are used, then there is the possibility that the flow direction in some cells cannot be defined. To overcome this problem, Tarboton uses special treatments for such cells. The iterative process (based on Tarboton) implemented by us only uses the basic rules without any improvement and this can be a reason of why the water accumulation zones from the picture in the middle are so spread out.

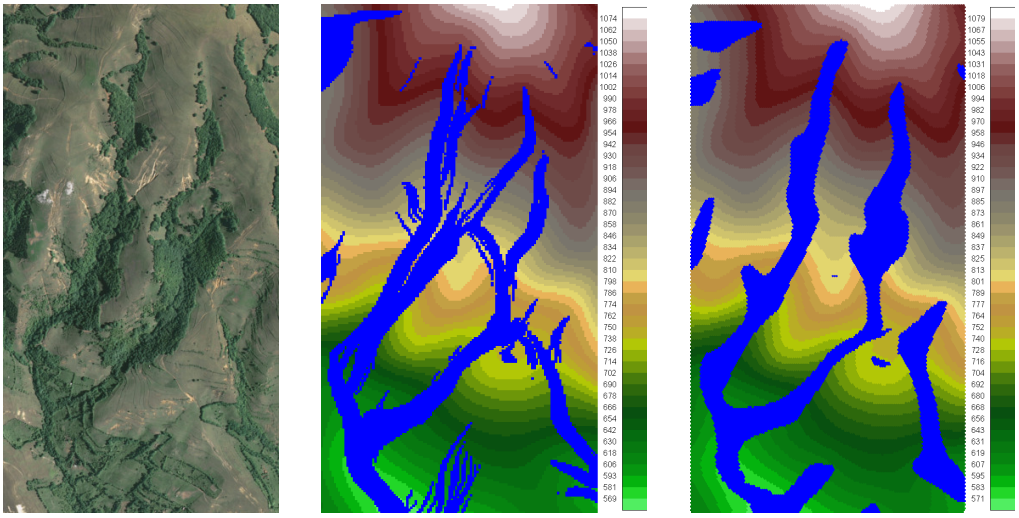

Figure 10: Potential water accumulation zones in Paul's Valley. The left figure is a photo of this region taken from the airplane. The relief from the image in the middle is given by the same 130×240 GIS raster data with square cells of 10 m size used for the middle picture from Figure 6. The relief from the right picture is generated from the hexagonal raster (of 5.7735 m cell size) obtained by applying ENO DP to the same GIS raster used for the middle image. The blue transparent areas represent the potential water accumulation zones determined by an iterative process of type (17). The picture in the middle is obtained using Tarboton's rules for water change among cells. For the picture on the right side, we used our water routing method described in this section. One clearly observes that the accumulation zones indicated by this method overlap almost perfectly the ravines and are less spread than the ones identified in the middle image.

5 Conclusions and Remarks

We provided a method for porting rectangular raster data on to hexagonal raster. The basic idea of the algorithm is to use an intermediate function

$\widetilde{g}$ that interpolates the rectangular raster function g^r and then define the hexagonal raster function g^h as the point values of $\widetilde{g}$ at the center of the hexagonal cell. The interpolation method can be extended to a less regular grid and can be also used (see A) to recover missing data or to filter outliers. Using some theoretical as well as some practical examples, we show that the extension function is closer to the function represented by raster data than raster function itself. As comparing to a well known cubic spline interpolant (CRS), Catmull-Rom (see Figure 5), ENO and CRS method have the same degree of accuracy, but CRS is faster than ENO method, and furnishes a smooth function in contrast with almost continuous function obtained by ENO method (see also Remark 1 in A for more theoretical details). The main argument for using ENO instead of CRS is that ENO method does not introduce spurious oscillations for cases of data with large gradients and works on a less regular grid points. For the case of digital terrain model, it is crucial to preserve the terrain shape and not to introduce artifacts. Both methods also provide a good compromise between a reduced amount of computational effort and the accuracy of the extended function.

The OF is an *unsupervised* outlier detection method and tries to recognize an abnormal point in a well defined neighborhood by evaluating the variation of the bicubic interpolant polynomials; an outlier is then detected since it introduces a larger variation than the neighboring regular points do. The method assumes some "smoothness" on these regular points and a certain sparsity of the outlier distributions. We point out that OF eliminates a detected outlier from the set of data used in the interpolation algorithm. The theoretical example presented in Section 4.1 and other data simulations not included in this paper encourage us to step further into this direction.

Table 4 compares features of our methods (ENO, OF), CRS, and Id (the extension function of Id is identical to the raster function). The numbers from the accuracy column represent the maximal degree of polynomials which can be exactly reconstructed. The property of recovering polynomials is closely related to the approximation order of the method. Data Recovery means the capability of the method to supply the missing data from a raster; an example of numerical errors in this matter is presented in Table 2. Row like grids can be pictured as points being arranged along parallel lines; for a mathematical definition, see A. The fidelity feature refers to the capacity of the method to preserve the qualitative shape of the function one has to reconstruct (the fidelity of a method should not be confused with the accuracy, see Figure 5 for two pictures of same accuracy but different shapes); the Id extension

function keeps the shape of the point distribution. A ranking of the methods from the speed point of view is given in the last column, 1 for the fastest.

Table 4: The main features of the interpolation methods discussed in this paper.

Method	Accuracy	Data Recovery	Grid	Fidelity	Outlier Detection	Speed (rank)
ENO	3	Yes	row like	high	No	3
OF	3	Yes	row like	unknown	Yes	3
CRS	3	No	regular	medium	No	2
Id	0	No	any	neutral	No	1

The water routing method presented in the Section 4.2 has a physical base and it is a simplified version of a discrete form of shallow water equations. One of the advantage of this approach is the use of hexagonal raster that benefits from the higher isotropy of hexagonal cells which allow a more suitable modelling of the transport phenomena. Another advantage of this approach is that it can be incorporated in more elaborated water flow models as a first step for a very quick investigation of the terrain topography and the potential water accumulation.

Further research directions include:

1. To develop the software in order to be compatible with variables having restrictions on the size and form of the discretization unit as a result of the observation scale and method.
   (a) to add other tessellations and irregular partitions, exposed as configurable user inputs;
   (b) to compute the value for each polygon in the plane partition in two variants: at its center and by the average value of the intermediate function in the polygon, exposed as configurable user inputs;
   (c) to develop an algorithm for nominal DP.
2. To construct a user friendly interface for the DP tool.
3. To develop a multiresolution analysis by using cubic spline wavelets in order to examine the GIS data (data de-noising and compression will be also considered).

Remarks Concerning the Asterix Porting Data Software

- The downloadable version of the Asterix Porting Data Software available on the web is part of a larger package in development. The current version contains the ENO scheme, the construction of a hexagonal raster, and the DP from a GIS to a hexagonal raster. In addition, a tool for plotting the hexagonal raster is also included.
- This version does not contain examples of all the theoretical and numerical results from the article. Readers who are interested in these examples are asked to email the authors.
- The software is available under GPL license and contains the necessary documentation for its usage.

Acknowledgment

This work was performed within the project 50/2012 ASPABIR (www.aspabir.biogeochemistry.ro) funded by Executive Agency for Higher Education, Research, Development and Innovation Funding, Romania (UEFISCDI). The authors acknowledge Florian Bodescu, who provided the digital terrain model. They specially thank all four anonymous reviewers for the constructive criticism that greatly improved the manuscript.

A Essentially Non-Oscillating Extension Algorithm

Here we present some details about the ENO algorithm and we extend it to a less regular net of points. Let $\mathcal{D}$ be a rectangular domain

$$\mathcal{D} := \{(x, y) \in \mathbb{R}^2 \mid a \leq x \leq b,\ c \leq y \leq d\},$$

where a, b, c, d are some arbitrarily fixed real numbers. We call a *row like grid* in $\mathcal{D}$ any set $\mathcal{N}$ of the form

$$\mathcal{N} := \{P_{i,j} = (x_i^j, y_j) \in \mathcal{D} \mid i = \overline{1, N_j},\ j = \overline{1, M}\}, \tag{18}$$

where $a <= x_1^j < \ldots < x_{N_j}^j <= b$ for all $j = \overline{1, M}$ and $c <= y_1 < \ldots < y_M <= d$. Note that the net has a variable number of knots on the lines $y = y_j$ and distance between two consecutive y_k and y_{k+1} is also variable.

Let $\mathbb{L}^\infty(\mathcal{D})$ be the space of bounded functions on $\mathcal{D}$ and $\mathcal{R} := \{g : \mathcal{N} \to \mathbb{R}\}$ the space of reticulated functions. One defines the restriction

operator $\mathbf{R} : \mathbb{L}^\infty(\mathcal{D}) \to \mathcal{R}$ by $\mathbf{R}(G)(P_{i,j}) = G(P_{i,j})$ for all $P_{i,j} \in \mathcal{N}$. We call $\mathbf{L} : \mathcal{R} \to \mathbb{L}^\infty(\mathcal{D})$ the extension operator.

To find the extension polynomial at an interval I_k^ξ, one needs to solve the minimization problem (6) which involves the calculation of the quantity

$$d_{p,q}^k := \left\| \mathcal{P}_{(k,k+1)}^{f;(p,q)} - \mathcal{Q}_k^f \right\|_{\mathbb{L}^2(I_k^\xi)}^2. \tag{19}$$

By standard calculation, we have

$$d_{p,q}^k = c \cdot \Big((\lambda_{p,q}^k)^2 + (\mu_{p,q}^k)^2 + 3/2 \cdot \lambda_{p,q}^k \mu_{p,q}^k \Big), \tag{20}$$

where

$$\begin{aligned} \delta_{p,q}^k &= (\xi_{k+1} - \xi_k)[\xi_k; \xi_{k+1}; \xi_p; \xi_q] f, \\ \lambda_{p,q}^k &:= \frac{\xi_k - \xi_p}{\xi_{k+1} - \xi_k} \delta_{p,q}^k + [\xi_k; \xi_{k+1}; \xi_p] f, \\ \mu_{p,q}^k &:= \lambda_{p,q}^k + \delta_{p,q}^k. \end{aligned} \tag{21}$$

and c is a constant independent of the knots p and q. Using (20) and (21), the minimization step in the algorithm (6) can be reformulated as:

$$\begin{aligned} &\text{Find } i, j \text{ s.t. } \{(\xi_i, \xi_j)\} = \arg\min_{\xi_p, \xi_q} d_{p,q}^k, \\ &\text{with the pair } (p,q) \in \{(k-2, k-1), (k-1, k+2), (k+2, k+3)\}. \end{aligned} \tag{22}$$

Let $\mathbf{l}_\xi$ stand for the 1D continuous extension operator from the space of reticulated functions to the space of continuous functions. The algorithm to evaluate the 1D extension operator $\mathbf{l}_\xi$ read as:

Algorithm 1. The 1D ENO Algorithm

Data Input: $\{\xi_i\}_{i=\overline{1,N}}$, $f : \{\xi_i\}_{i=\overline{1,N}} \to \mathbb{R}$; ξ.
Data Output: $\mathbf{l}_\xi(f)(\xi)$.

1. Find I_k^ξ such that $\xi \in I_k^\xi$.
2. Define S_k^ξ of the form (5).
3. Find the knots ξ_i, ξ_j using (22).
4. Set $\mathbf{l}_\xi(f)(\xi) := \mathcal{P}_{(k,k+1)}^{f;(i,j)}(\xi)$.

Note that the extension 1D ENO algorithm can also be applied for the points ξ outside the interval $[\xi_1, \xi_N]$, using the following formula

$$\mathbf{l}_\xi(f)(\xi) = \begin{cases} \mathcal{P}_{(1,2)}^{f;(3,4)}(\xi), & \text{for} \quad \xi < \xi_1 \\ \\ \mathcal{P}_{(N-1,N)}^{f;(N-3,N-2)}(\xi), & \text{for} \quad \xi > \xi_N \end{cases} . \tag{23}$$

Now, having the 1D ENO scheme (22) and (23), one can set up the algorithm to define the 2D extension operator $\mathbf{L}$.

Algorithm 2. The 2D ENO Algorithm

Data Input: $\mathcal{D}, \mathcal{N}, g : \mathcal{N} \to \mathbb{R}; (x, y) \in \mathcal{D}$
Data Output: $\mathbf{L}(g)(x, y)$.

1. Find I_k^y such that $y \in I_k^y$.
2. Define S_k^y of the form (5).
3. For each m s.t. $y_m \in S_k^y$, using Algorithm 1, calculate
$$f_m(x) := \mathbf{l}_x(g(\cdot, y_m))(x)$$
4. Set $\mathbf{L}(g)(x, y) := \mathbf{l}_y(f(x, \cdot))\Big|_{I_k^y}(y)$.

In this algorithm, $\mathbf{l}_x$ and $\mathbf{l}_y$ denotes the 1D extension operators with respect to Ox and Oy knots, respectively. The notation $\mathbf{l}_x(g(\cdot, y_m))$ from

Step 3 reads as follows: the extension operator $\mathbf{l}_x$ acts on the reticulated function $g(\cdot, y_m)$ having the values $g(x_i^m, y_m)$ on the Ox knots $\{x_i^m\}_{i=1,N_m}$. Also, $f(x,\cdot)$ from Step 4 represents the reticulated function having the values $f(x, y_m) = f_m(x)$ on the Oy knots $y_m \in S_k^y$.

Remark 1 *Essentially, the 2D ENO extension operator* $\mathbf{L}$ *is given by*

$$\mathbf{L}(g) := (\mathbf{l}_y \circ \mathbf{l}_x)(g).$$

For the 2D ENO extension function the following properties hold:

1. $\mathbf{L}(g)(P_{ij}) = g(P_{ij})$, *for all* $g \in \mathcal{R}$.
2. $\mathbf{L}(G)$=G, *for all* $G \in \pi_{3,3}$
3. $\mathbf{L}(g)$ *is always continuous with respect to* y *and continuous with respect to* x *except for a finite number of points.*
4. *If when on Step 4 of Algorithm 2 the problem* (22) *does not have a unique solution for a particular* x, *then* (x, y) *is possibly a discontinuity point of the extension function* $\tilde{g}$. *Otherwise,* $\tilde{g}$ *is locally continuous at* (x, y).

Remark 2 *Algorithm 1 and Algorithm 2 can be easily adapted for the OF interpolation method.*

B Details on test rasters from Section 4.1.2

The test rasters we used in Section 4.1.2 are constructed as it follows.

Let δ be the cell size of the square basis raster, and m, n some positive integers. In order to construct a square test raster, we randomly eliminate rows of cells except the top and bottom rows, such that the distance between any two consecutive remaining rows does not exceed $m\delta$. Then, for each of the remaining rows, we randomly eliminate cells except the first and last ones, such that the distance between any two consecutive remaining cells does not exceed $n\delta$. The Figure 11 gives the correspondence between the test index α and the parameters m, n, and an example of a possible point distribution of the kept data in the grid for such test.

α	m	n
1	3	3
2	4	3
3	5	3
4	5	4
5	5	5

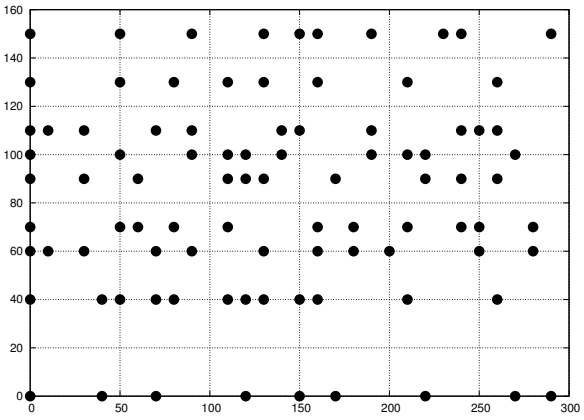

Figure 11: The correspondence between the test raster index α and the parameters m, n, and a snapshot example (the lower left corner) of a point distribution in the grid for $\alpha = 5$ and $\delta = 10$ m.

References

[1] J. M. Baetens, D.K. Loof, and D. B. Baets. Influence of the topology of a cellular automaton on its dynamical properties. *Commun. Nonlinear Sci. Numer. Simulat.*, 18:651–668, 2013.

[2] Colin P.D. Birch, Sander P. Oom, and Jonathan A. Beecham. Rectangular and hexagonal grids used for observation, experiment and simulation in ecology. *Ecological Modelling*, 206:347–359, 2007.

[3] John M. Chambers. *Software for Data Analysis: Programming with R.* Springer, 2008.

[4] N. Chiba, K. Muraoka, and K. Fujita. An erosion model based on velocity fields for the visual simulation of mountain scenery. *Journal of Visualization and Computer Animation*, 9:185–194, 1998.

[5] Noel A. C. Cressie. *Statistics for Spatial Data.* Wiley, revised edition edition, January 1993.

[6] D. D'Ambrosio, S. Di Gregorio, S. Gabriele, and R. Gaudio. A cellular automata model for soil erosion by water. *Physics and Chemistry of the Earth, Part B: Hydrology, Oceans and Atmosphere*, 26(1):33–39, 2001.

[7] D. D'Ambrosio, S. Di Gregorio, S. Gabriele, and R. Gaudio. Il modello ad automi cellulari scavatu per la simulazione dell'erosione del suolo e del trasporto solido nei bacini idrografici: specificazione della parte idrodinamica nel caso di reticolo a celle esagonali regolari. Technical Report 586, Consiglio Nazionale delle Ricerche Istituto di Ricerca per la Protezione Idrogeologica, giugno 2002.

[8] Luís de Sousa, Nery Fernanda, Sousa Ricardo, and Matos João. Assessing the accuracy of hexagonal versus square tiled grids in preserving DEM surface flow directions. In *Proceedings of the 7th International Symposium on Spatial Accuracy Assessment in Natural Resources and Environmental Sciences (Accuracy 2006)*, pages 191–200. Instituto Geográphico Português, 2006.

[9] Neil Antony Dodgson. Image resampling. Technical Report UCAM-CL-TR-261, University of Cambridge, Computer Laboratory, August 1992.

[10] Olivier Dubrule. Two methods with different objectives: Splines and kriging. *Journal of the International Association for Mathematical Geology*, 15(2):245–257, 1983.

[11] Shelly Eberly, Jenise Swall, David Holland, Bill Cox, and Ellen Baldridge. Developing spatially interpolated surfaces and estimating uncertainty. Technical Report EPA-454/R-04-004, Office of Air Quality Planning and Standards, Office of Air and Radiation, U.S. Environmental Protection Agency, November 2004.

[12] David Favis-Mortlock, Tony Guerra, and John Boardman. A self-organizing dynamic systems approach to hillslope rill initiation and growth: model development and validation. In W. Summer, E. Klaghofer, and W. Zhang, editors, *Modelling Soil Erosion, Sediment Transport and Closely Related Hydrological Processes*, pages 53–62. IAHS Publication no. 249, July 1998.

[13] Mark A. Fonstad. Cellular automata as analysis and synthesis engines at the geomorphology ecology interface. *Geomorphology*, 77:217–234, 2006.

[14] U. Frisch, B. Hasslacher, and Y. Pomeau. Lattice-gas automata for the navier-stokes equation. *Phys. Rev. Lett.*, 56:1505–1508, Apr 1986.

[15] Thierry Gallouet, Jean-Marc Herard, and Nicolas Seguin. Some approximate godunov schemes to compute shallow-water equations with topography. *Computers & Fluids*, 32(4):479–513, 2003.

[16] Antony Galton. Fields and objects in space, time, and space-time. *Spatial Cognition and Computation*, 1:39–68, 2004.

[17] R. H. Gardner, T. R. Lookingbill, P. A. Townsend, and J. Ferrari. A new approach for rescaling land cover data. *Landscape Ecology*, 23:53–526, 2008.

[18] M. F. Goodchild. Geographical data modeling. *Computers and Geosciences*, 8:401–408, 1992.

[19] M. C. Gough and S. P. Rushton. The application of gis-modelling to mustelid landscape ecology. *Mammal Rev.*, 30:197–216, 2000.

[20] Julian Hagenauer and Marco Helbich. Contextual neural gas for spatial clustering and analysis. *International Journal of Geographical Information Science*, 27(2):251–266, 2013.

[21] Ami Harten, Bjorn Engquist, Stanley Osher, and Sukumar R Chakravarthy. Uniformly high order accurate essentially non-oscillatory schemes, iii. *Journal of Computational Physics*, 71(2):231–303, August 1987.

[22] Ami Harten, Stanley Osher, Bjrn Engquist, and Sukumar R. Chakravarthy. Some results on uniformly high-order accurate essentially nonoscillatory schemes. *Applied Numerical Mathematics*, 2:347–377, October 1986.

[23] Amy Hillier. Manual for working with arcgis 10, 2011.

[24] E. E. Holmes, M. A. Lewis, J. Banks, and R. R. Veit. Partial differential equations in ecology: spatial interactions and population dynamics. *Ecology*, 75:17–29, 1994.

[25] M. F. Hutchinson. A new procedure for gridding elevation and stream line data with automatic removal of spurious pits. *Journal of Hydrology*, 106:211–232, 1989.

[26] Stelian Ion and Dorin Marinescu. Spline wavelets analysis of reticulated functions on bounded interval. *Mathematical Reports*, 4(2):191–205, 2002.

[27] V. Iordache, S. Ion, and A. Pohoata. Integrated modeling of metals biogeochemistry: potential and limits. *Chem Erde Geochem*, 69:125–169, 2009.

[28] V. Iordache, E. Kothe, A. Neagoe, and F. Gherghel. A conceptual framework for up-scaling ecological processes and application to ectomycorrhizal fungi. In M. Rai and A. Varma, editors, *Diversity and biotechnology of ectomycorrhizae*, pages 255–299. Springer, 2011.

[29] V. Iordache, R. Lacatusu, D. Scradeanu, M. Onete, D. Jianu, F. Bodescu, A. Neagoe, D. Purice, and I. Cobzaru. Contributions to the theoretical foundations of integrated modeling in biogeochemistry and their application in contaminated areas. In E. Kothe and A. Varma, editors, *Bio-geo interactions in metal-contaminated soils*, volume 31, pages 385–416. Springer, 2012.

[30] Bin Jiang. Extraction of spatial objects from laser-scanning data using a clustering technique. In *XXth ISPRS Congress: Geo-Imagery bridging continents*, volume 3, pages 219–224, 2004.

[31] J. Kumhálová, F. Kumhála, P. Novák, and Š Matějková. Airborne laser scanning data as a source of field topographical characteristics. *Plant, Soil and Environment*, 59(9):423–431, 2013.

[32] Seungyong Lee, George Wolberg, and Sung Yong Shin. Scattered data interpolation with multilevel b-splines. *IEEE Transactions on Visualization and Computer Graphics*, 3(3):228–244, July-September 1997.

[33] Thomas M. Lehmann, Claudia Gonner, and Klaus Spitzer. Survey: interpolation methods in medical image processing. *IEEE Transactions on Medical Imaging*, 18:1049–1075, November 1999.

[34] David J. C. MacKay. Bayesian interpolation. *Neural Computation*, 4:415–447, 1992.

[35] G. Matheron. Splines and Kriging; their formal equivalence. In D. F. Merriam, editor, *Down-to-Earth Statistics: Solutions looking for Geological Problems*, pages 77–95. Syracuse University Geology Contributions, 1981.

[36] L. Mitas and H. Mitasova. Spatial interpolation. In P. Longley, M. F. Goodchild, D. J. Maguire, and D. W. Rhind, editors, *Geographical Information Systems: Principles, Techniques, Management and Applications*, volume 1, pages 481–492. Wiley, 1999.

[37] Don P. Mitchell and Arun N. Netravali. Reconstruction filters in computer-graphics. *SIGGRAPH Comput. Graph.*, 22(4):221–228, June 1988.

[38] Jane Molofsky and James D. Bever. A new kind of ecology? *BioScience*, 54(5):440–446, 2004.

[39] I. D. Moore, R. B. Grayson, and A. R. Ladson. Digital terrain modelling: a review of hydrological, geomorphological, and biological applications. *Hydrological Processes*, 5:3–30, 1991.

[40] Eder Paulo Moreira, W.J. Elliot, and A.T. Hudak. Effects of dtm resolution on slope steepness and soil loss prediction on hillslope profiles. In *The XXXIII Brazilian Congress of Soil Science symposium, Soils: Climate change and sustainability*, 2011.

[41] John F. O'Callaghan and David M. Mark. The extraction of drainage networks from digital elevation data. *Computer Vision, Graphics, and Image Processing*, 28(3):323–344, 1984.

[42] Jon D. Pelletier. Minimizing the grid-resolution dependence of flow-routing algorithms for geomorphic applications. *Geomorphology*, 122(1-2):91–98, 2010.

[43] P. Quinn, K. Beaven, P. Chevallier, and O. Planchon. The prediction of hillslope flow paths for distributed hydrological modelling using digital terrain models. *Hydrological Processes*, 5(1):59–79, 1991.

[44] K. Sahr. Hexagonal discrtete global grid systems for geospatial computing. *Archives of Photogrammetry, Cartography and Remote Sensing*, 22:363–376, 2011.

[45] I.J. Schoenberg. *Cardinal Spline Interpolation*, volume CBMS-NSF Regional Conference Series in Applied Mathematics 12. Capital City Press, Montpelier, Vermont, second printing edition, 1993.

[46] Jan Seibert and Brian L. McGlynn. A new triangular multiple flow direction algorithm for computing upslope areas from gridded digital elevation models. *Water Resources Research*, 43(4), 2007.

[47] Elisabete A. Silva, Jack Ahern, and Jack Wileden. Strategies for landscape ecology: An application using cellular automata models. *Progress in Planning*, 70:133–177, November 2008.

[48] S. L. Smith, D. A. Holland, and P. A. Longley. The importance of understanding error in lidar digital elevation models. *International Archives of the Photogrammetry, Remote Sensing and Spatial Information Sciences*, 35:996–1001, 2004.

[49] Pierre Soille, Jrgen Voght, and Roberto Colombo. Carving and adaptive drainage enforcement of grid digital elevation models. *Water Resources Research*, 39(12):1366–1375, 2003.

[50] Shruthi Srinivasan, Sorin C. Popescu, Marian Eriksson, Ryan D. Sheridan, and Nian-Wei Ku. Multi-temporal terrestrial laser scanning for modeling tree biomass change. *Forest Ecology and Management*, 318(0):304–317, 2014.

[51] Christoph Stasch, Simon Scheider, Edzer Pebesma, and Werner Kuhn. Meaningful spatial prediction and aggregation. *Environmental Modelling&Software*, 51:149–165, 2014.

[52] David G. Tarboton. A new method for the determination of flow directions and upslope areas in grid digital elevation models. *Water Resources Research*, 33(2):309–319, 1997.

[53] C. Varekamp, A. K. Skidmore, and P. A. B. Burrough. Using public domain geostatistical and gis software for spatial interpolation. *Photogrammetric Engineering and Remote Sensing*, 62(7):845–854, July 1996.

[54] R. F. Vazquez and J. Feyen. Assessment of the effects of dem gridding on the predictions of basin runoff using mike she and a modelling resolution of 600 m. *Journal of Hydrology*, 334:73–87, 2007.

[55] Alexey Voinov and Herman H. Shugart. 'integronsters', integral and integrated modeling. *Environmental Modeling&Software*, 39:149–158, 2013.

[56] J. P. Walker and G. R. Willgoose. On the effect of digital elevation model accuracy on hydrology and geomorphology. *Water Resources Research*, 35(7):2259–2268, 1999.

[57] Yu Wei, Xuemei Li, Jie Wang, Caiming Zhang, and Yi Liu. Graph cuts image segmentation in a hexagonal-image processing framework. *Journal of Computational Information Systems*, 8(14):5953–5960, 2012.

[58] Marco J. Van De Wiel, Tom J. Coulthard, Mark G. Macklin, and John Lewin. Embedding reach-scale fluvial dynamics within the caesar cellular automaton landscape evolution model. *Geomorphology*, 90:283–301, 2007.

[59] John P. Wilson, Christine S. Lam, and Yongxin Deng. Comparison of the performance of flow-routing algorithms used in gis-based hydrologic analysis. *Hydrological Processes*, 21(8):1026–1044, 2007.

[60] Dieter Wolf-Gladrow. *Lattice-gas cellular automata and lattice Boltzmann models an introduction*. Springer, 1st edition, March 2000.